Solar Phys (2011) 271:197–218
DOI 10.1007/s11207-011-9800-z

Straylight-Rejection Performance of the STEREO HI Instruments

J.-P. Halain · C.J. Eyles · A. Mazzoli · D. Bewsher · J.A. Davies · E. Mazy · P. Rochus · J.M. Defise · C.J. Davis · R.A. Harrison · S.R. Crothers · D.S. Brown · C. Korendyke · J.D. Moses · D.G. Socker · R.A. Howard · J.S. Newmark

Received: 23 February 2011 / Accepted: 17 May 2011 / Published online: 6 July 2011

Abstract The SECCHI Heliospheric Imager (HI) instruments on-board the STEREO spacecraft have been collecting images of solar wind transients, including coronal mass ejections, as they propagate through the inner heliosphere since the beginning of 2007.

The scientific use of the images depends critically on the performance of the instruments and its evolution over time. One of the most important factors affecting the performance of the instrument is the rejection of straylight from the Sun and from other bright objects located both within and outside the HI fields of view.

This paper presents an analysis of the evolution of the straylight-rejection performance of the HI instrument on each of the two STEREO spacecraft over the three first years of the mission. The straylight level has been evaluated and expressed in mean solar brightness units, in which such scientific observations are usually quoted, using photometric conversion factors.

J.-P. Halain (✉) · A. Mazzoli · E. Mazy · P. Rochus
Centre Spatial de Liège, Université de Liège, avenue Pré Aily, 4031 Angleur, Belgium
e-mail: jphalain@ulg.ac.be

C.J. Eyles
Laboratorio de Procesado de Imagenes, Universidad de Valencia, Valencia 46071, Spain

D. Bewsher · D.S. Brown
Jeremiah Horrocks Institute, University of Central Lancashire, Preston, Lancashire, PR1 2HE, UK

J.M. Defise
Institut d'Astrophysique et de Géophysique, Université de Liège, 4000 Liège, Belgium

C.J. Eyles · J.A. Davies · C.J. Davis · R.A. Harrison · S.R. Crothers
RAL Space, STFC Rutherford Appleton Laboratory, Chilton, Didcot, Oxfordshire OX11 0QX, UK

C. Korendyke · J.D. Moses · D.G. Socker · R.A. Howard · J.S. Newmark
Space Science Division, Naval Research Laboratory, Washington, DC, USA

J.S. Newmark
NASA Headquarters, 300 E Street, SW, M/S 3R15, Washington, DC 20546, USA

Keywords Straylight · Lens barrel rejection · Mean solar brightness · Off-pointing

1. Introduction

The *Solar Terrestrial Relations Observatory* (STEREO; Kaiser *et al.*, 2008) is a NASA mission comprising two near-identical spacecraft launched in October 2006 into Earth-like orbits, one leading (STEREO-A) and the other lagging (STEREO-B) the Earth.

The Sun Earth Connection Coronal and Heliospheric Investigation (SECCHI; Howard *et al.*, 2008) suite of remote-sensing instruments forms part of the STEREO payload. The SECCHI instruments observe solar wind transients such as coronal mass ejections (CMEs) as they propagate from the Sun out to 1 AU and beyond, including, most notably, those directed toward the Earth. The SECCHI suite on each STEREO spacecraft includes the Heliospheric Imager (HI), a wide-field, visible-light imaging system (Eyles *et al.*, 2009).

One of the most important aspects of HI instrument performance is the instrument straylight rejection. Straylight corresponds to a signal in the camera field of view coming indirectly from a light source or an illuminated surface located out of the field of view.

The Sun is the brightest source located out of the HI field of view and therefore represents the main potential straylight source in the HI instrument. Light from the Sun is attenuated by a multi-edges cascading diffractive HI front baffle (Defise *et al.*, 2001). The stars and planets within the instrument field of view are also potentially straylight sources as their intensities can be reflected by the instrument internal cavity. The design of the HI instrument is therefore based on a double-baffle system, providing a high level of rejection of straylight both from out-of-field sources (solar straylight) and in-field sources (stellar and planetary straylight). The baffles protect two optical systems named HI-1 and HI-2 (Figure 1), with 20- and 70-arcdeg fields of view off-pointed from Sun-center by 14.0 and 53.7 arcdeg, respectively.

The straylight performance of the HI front and internal baffles was modeled, and the front baffle efficiency measured, during the instrument development (Defise *et al.*, 2002). On-ground end-to-end validation was performed and compared with early in-flight measurements showing the high level of straylight attenuation achieved by the HI baffle system (Halain *et al.*, 2007). The present paper develops this work further by investigating the evolution of the straylight-rejection performance of the two HI instruments over the three first years of the STEREO mission.

To derive quantitative results from the HI images, it is common to use a conversion factor to convert from the detector measurement in units of DN s^{-1} px^{-1} to a measure of the true intensity. The mean solar brightness unit (B_0) is generally considered as the most appropriate unit of radiance in terms of the phenomena of interest here (*i.e.* solar wind transients), and it is independent of the wavelength.

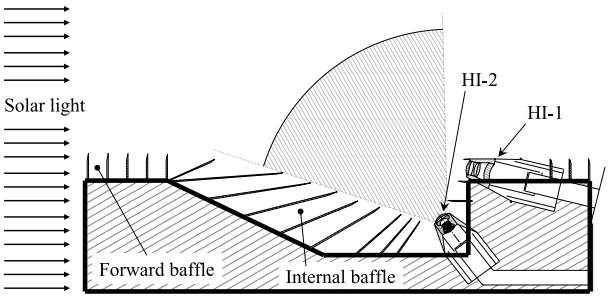

Figure 1 HI instrument overview, showing the instrument baffles and the two cameras.

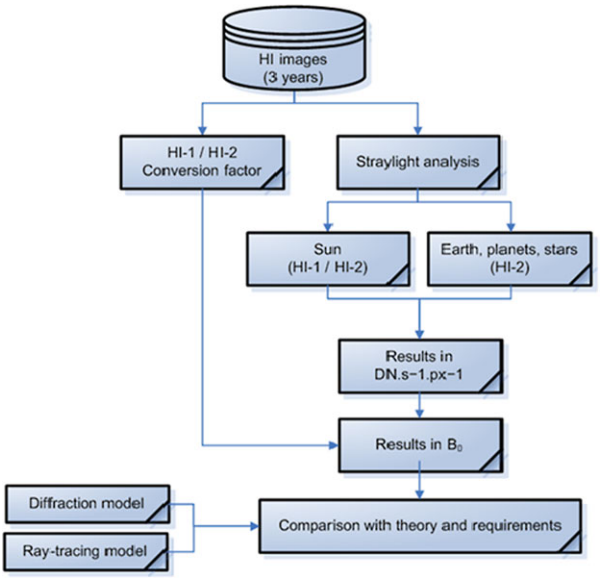

Figure 2 Work flow of the straylight performance evaluation.

The work flow used to evaluate the straylight performance is presented in Figure 2. Starting from in-flight images and conversion factors, the straylight analysis is conducted in order to derive results expressed in unit of B_0 that are subsequently compared with instrument theoretical diffraction and ray-tracing models, and with the instrument straylight requirements.

2. Conversion Factor

Preliminary conversion factors were produced by Mazy *et al.* (2005) from the pre-flight calibration of the HI instruments. These were used to compute the straylight level at the start of the mission in order to confirm the solar rejection performance (Halain *et al.*, 2007). The pre-flight characterization of the response of the HI instrument was performed using a calibrated laser diode in the spectral range of the optical systems, *i.e.* 630 – 730 nm for HI-1 and 400 – 1000 nm for HI-2. This provided a preliminary factor for converting the data output by the instrument into physical units (DN to nJ or, equivalently, DN to photons at the 670 nm central bandpass wavelength) (Mazy *et al.*, 2005). However, due to setup artifacts, the results of the first calibration (HI-A) were not sufficiently reliable and thus the setup was improved for the HI-B calibration. With both HI instruments being identical to a first approximation, the HI-B calibration results were assumed applicable to HI-A.

Accurate post-launch conversion factors have since been obtained for HI-1A and HI-1B (Bewsher *et al.*, 2010). The method of Bewsher *et al.* (2010) is repeated here to obtain preliminary conversion factors for the HI-2 cameras. It consists of two parts:

- Determination of a factor that converts from predicted stellar intensity, F (determined by folding stellar spectra (Pickles, 1998) through the HI instrument response), to the measured stellar intensity, I (determined from aperture photometry). This is represented by their Equation (6): $I = \mu F$.
- Folding a solar spectrum (Neckel and Labs, 1984) through the HI instrument response to determine the predicted HI instrument solar response, and then adjusting, using the factor

Table 1 HI in-flight conversion factor [B_0/DN s^{-1} px^{-1}]. The in-flight conversion factors for the HI-1 cameras are those given in Bewsher *et al.* (2010), and the values for the HI-2 cameras are derived following the procedure of Bewsher *et al.* (2010), who used the total DN s^{-1} per pixel in the 2 × 2 binned science images. In the case of data which have been through secchi_prep these factors must be multiplied by four, since in this case the intensities are converted to units of DN s^{-1} per CCD pixel.

	HI-1A	HI-1B	HI-2A	HI-2B
Pre-flight (Mazy *et al.*, 2005)	7.5×10^{-14}		1.7×10^{-14}	
In-flight	8.99×10^{-14}	9.04×10^{-14}	1.07×10^{-14}	1.14×10^{-14}

calculated above, to simulate what the solar intensity measured by the instrument would be. This is used to calculate the conversion factor in mean solar brightness units.

The determination of μ is out of the scope of this paper. However, for the HI-1 cameras, μ was shown to be very close to 1 (0.93 for HI-1A and 0.98 for HI-1B, Bewsher *et al.*, 2010). Therefore, for this work, it is assumed that $\mu = 1$ for the HI-2 cameras. Physically this means that the stellar spectrum folded through the HI-2 instrument response is assumed to provide a perfect prediction of what the HI-2 cameras would actually measure using aperture photometry.

The equations in Section 3.7.1 of Bewsher *et al.* (2010) are used to calculate the mean solar brightness conversion factor, and are given here for completeness. The conversion factor from DN s^{-1} px^{-1} to B_0 for a diffuse source is given by

$$C_{\mathrm{MSB}} = \frac{n_{\mathrm{pix}}}{I_0},$$

where I_0 is the predicted total intensity of the Sun in DN s^{-1} if it were to be imaged by the instrument, and n_{pix} is the number of pixels imaging the solar disk and is given by

$$n_{\mathrm{pix}} = \frac{\pi\left(\frac{D_0}{2}\right)^2}{D_{\mathrm{pix}}^2},$$

where D_0 is the mean angular diameter of the Sun and D_{pix} is the angular pixel scale. As in Bewsher *et al.* (2010), the mean angular diameter of the Sun (D_0) is taken to be 32 arcmin. The number of pixels needed to image the solar disk (n_{pix}) would be 42.8 and 43.0 at the center of the field of view for HI-2A and HI-2B, respectively. Table 1 presents the in-flight conversion factors determined by Bewsher *et al.* (2010) for the HI-1 cameras, the preliminary conversion factors for HI-2 cameras determined using the method detailed above and the pre-flight values derived by Mazy *et al.* (2005).

3. Straylight Performance

To ensure that the scientific measurements made by an imaging instrument are not contaminated by unwanted light, it is vital to have a good characterization of the straylight incident upon its detector. The level of straylight must be sufficiently lower than the signal of scientific interest, and, moreover, understanding its evolution over time is of critical importance.

In this paper, the straylight in the case of both the HI-1 and HI-2 cameras has been evaluated and its evolution since the beginning of the mission has been characterized. Based on the in-flight conversion factors discussed in the previous section, the straylight levels in HI-1 and HI-2 have been converted to unit of B_0.

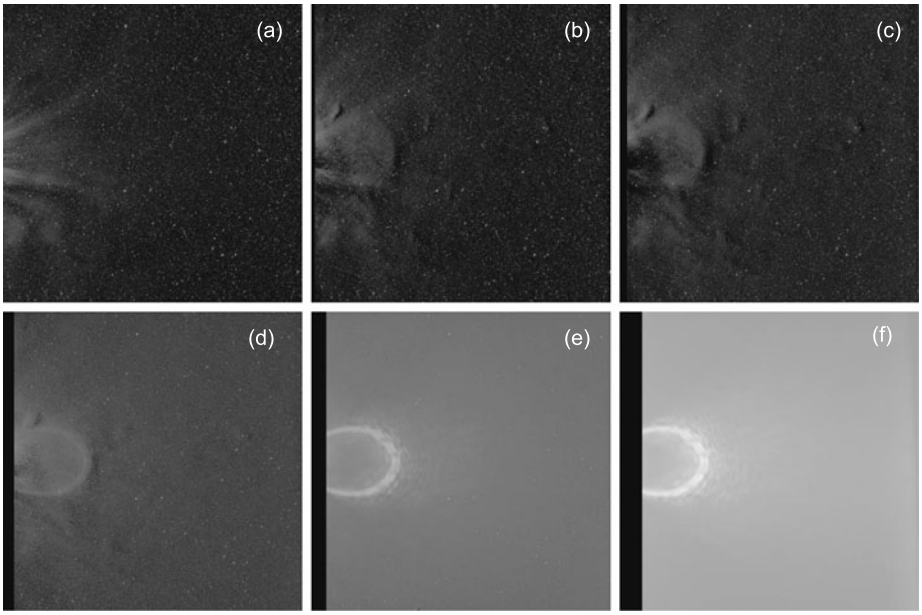

Figure 3 Background-subtracted HI-1B in-flight images (May 2010) for increasing pitch off-points (a) 0 arcdeg, (b) −0.25 arcdeg, (c) −0.5 arcdeg, (d) −0.75 arcdeg, (e) −1.00 arcdeg, (f) −1.25 arcdeg. Negative off-points are toward the Sun which, here for HI-B, is off the left-hand side of the image.

3.1. HI-1 Straylight Analysis

The major contributor of straylight to the HI instruments, in particular for HI-1, is the Sun. Light from the Sun is attenuated by the front baffle's cascading diffractive 5-edges (Defise *et al.*, 2001). The theoretical curve for the rejection of sunlight by this front baffle system had been computed based on Fresnel diffraction laws, and its rejection efficiency has been validated by on-ground tests (Defise *et al.*, 2002; Mazy *et al.*, 2005; Halain *et al.*, 2007).

The in-flight level of solar straylight for HI-1, based on 30 January 2007 pitch off-pointed images and computed using the on-ground conversion factor, showed a good agreement with theoretical values (Halain *et al.*, 2007).

This comparison has been redone using the in-flight HI-1 conversion factor computed by Bewsher *et al.* (2010), and extended with the use of new off-pointed images obtained in May 2010 (Figure 3).

3.1.1. Theoretical Straylight

The HI-1 theoretical straylight curve therefore includes a model of multi-edges cascading diffraction (Figure 4) by the front baffle (Defise *et al.*, 2002) for a 13.65-arcdeg pointing relative to Sun-center, also assuming an out of the field of view lens barrel rejection of 1×10^{-2}. This value for the lens barrel rejection is an average value over the HI-1 CCD detector (27.65 mm × 27.65 mm) extrapolated from out-of-field measurements on a 10 mm^2 single pixel photodiode (performed during the instrument development, and discussed by Mazy *et al.*, 2005), the closest value next to the field of view border being considered (Figure 5).

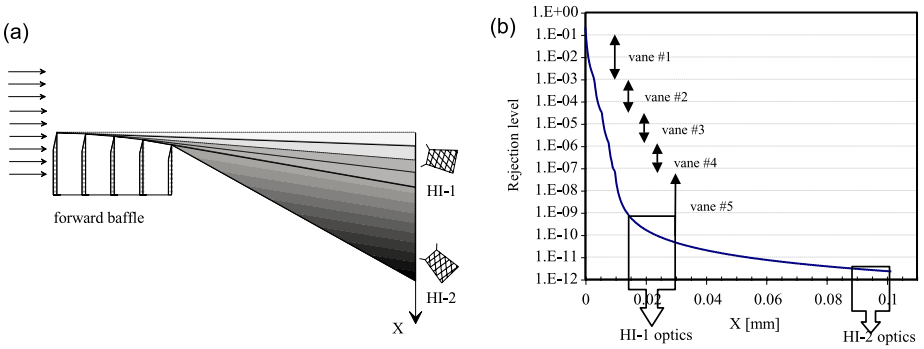

Figure 4 HI front baffle concept with location of the HI-1 and HI-2 optical systems (a) and the theoretical curve of cascading diffraction efficiency of the multi-edges front baffle (b).

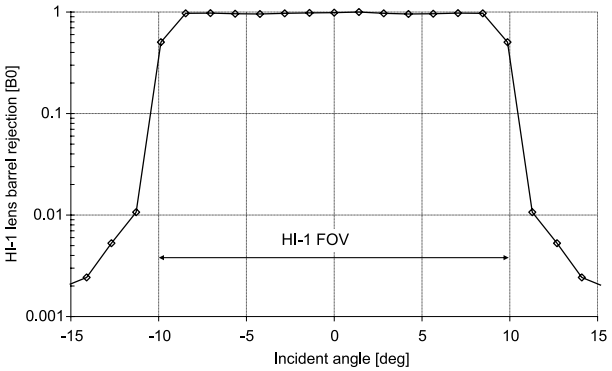

Figure 5 HI-1 lens barrel rejection curve, extrapolated from Mazy *et al.* (2005) obtained using a 10 mm^2 single pixel photodiode.

3.1.2. Comparison of In-Flight Versus Theoretical Straylight for HI-1

The in-flight off-pointed images from January 2007 were taken at instrument pointing angle of -0.25, -0.5, -0.75, -1.00 and -1.50 arcdeg in pitch, progressively shifting the image toward the Sun. In May 2010, similar off-pointed images were taken, except that the largest off-point was -1.25 arcdeg instead of -1.5 arcdeg in order to limit the image saturation. Additionally, off-pointed images with positive pitch of $+0.5$ and $+1.0$ arcdeg were also taken (here the images are shifted away from the Sun).

The front baffle was designed for an HI-1 boresite offset at 13.65 arcdeg from Sun-center. To compare with the theoretical rejection curve it is therefore necessary to take into account the additional 0.33-arcdeg pitch angle offset that was added during the mounting of the HI instruments onto the STEREO spacecraft (Figure 6) to provide a margin in the straylight rejection of the front baffle above what was predicted theoretically, resulting in the 14-arcdeg nominal offset of the boresite. The images taken at -0.25 arcdeg are therefore the closest to the theoretical diffraction model and can be used to compare the measured straylight with theoretical predictions.

For each pixel within the images, an angle from the boresite is calculated taking into account the deviation from the gnomonic projection due to the wide-angle nature of the cameras, as described by Brown, Bewsher, and Eyles (2008).

The HI images on which we base our analysis are 1024×1024 binned images, calibrated using the Solar Soft SECCHI_PREP routine in order to *i*) correct for shutterless operations,

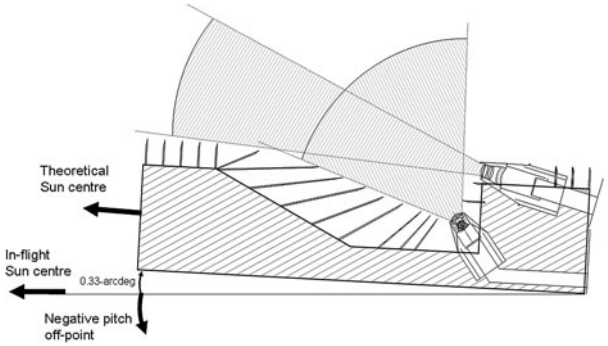

Figure 6 HI pitch angle pointing with respect to the Sun-center direction. An additional 0.33 arcdeg has been added to the HI-1 field of view pointing angle from the center of the Sun as compared to value considered in the front baffle model.

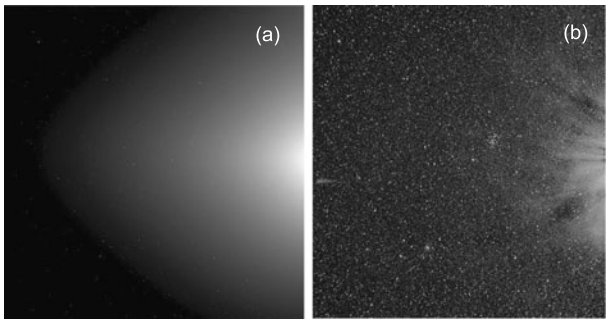

Figure 7 Example of a nominal-pointing HI-1A image pre (a) and post (b) background removal. The Sun is off the right-hand side of the image.

ii) take into account a flat-field correction (the SECCHI_PREP version used here applies a pre-flight flat-field), *iii*) calibrate the instrument pointing (see Brown, Bewsher, and Eyles, 2008) and *iv*) to weight images according to their exposure time (*i.e.* convert images from DN to DN s^{-1}). The processing ignores images containing bad areas (due to telemetry problem), and bad images (such as those contaminated by data from other STEREO instruments), and NaN values in images were not considered. A background is then removed from the images, as described in Eyles *et al.* (2009), by subtracting a background image computed using a minimum filter over nominal-pointing images taken on the off-pointing day. This background principally consists of the slowly varying F-corona with, to a lesser extent, a contribution due to the less-rapidly varying K-coronal components (the streamer belt). An example of such background removal is shown in Figure 7 and was applied for images of Figure 3.

For off-pointed images, the background removal is performed using the same method but shifting the background obtained at nominal pointing horizontally by the number of pixels corresponding to the off-point angle (Figure 8). No correction for the image distortion has been made when subtracting the shifted background images from the off-pointed images, because distortion is small in the HI-1 cameras ($\sim 1\%$ for the edge of the 10-arcdeg circular field of view and $\sim 2\%$ in the image corners). Furthermore, because the off-point angles are small compared to the size of the field of view, the difference in distortion (*i.e.* the relative plate-scale of the pixels) between pixels in the off-pointed image and those in the shifted background is negligible ($\ll 1\%$).

This results in a more accurate background subtraction but has the disadvantage of not providing values in the small region where the shifted background does not overlap with the image.

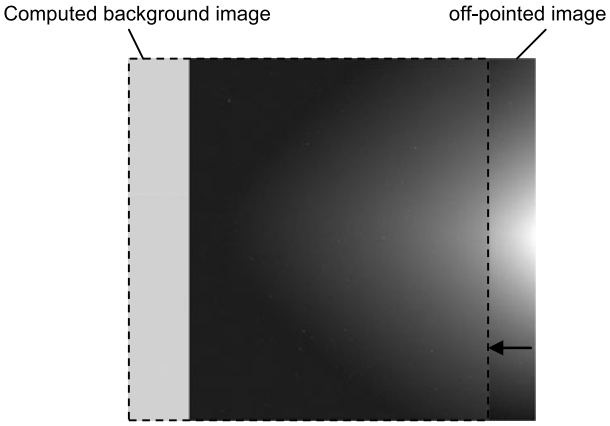

Figure 8 Example of background removal for off-pointed images where the background is shifted horizontally by the number of pixels corresponding to the off-point angle.

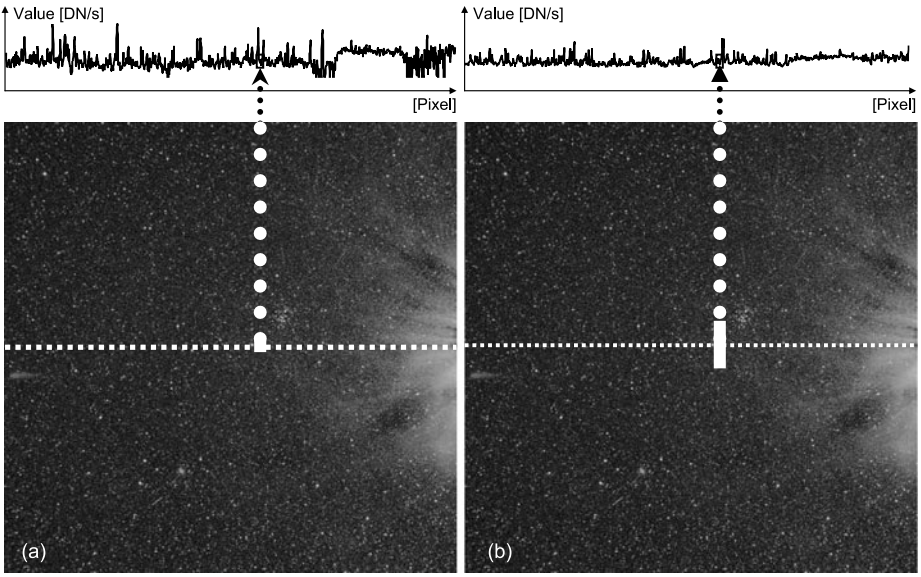

Figure 9 Example of the derivation of an in-flight data curve from an HI-1A processed image, for comparison with the theoretical straylight-rejection curve using (a) the image horizontal center line pixel values and (b) the image horizontal central strip.

An average over the four consecutive images captured for each off-pointing angle is also performed to reduce the noise in the darkest regions.

In the previous analysis, Halain *et al.* (2007) used in-flight data curves taken along the HI image horizontal center line (Figure 9a) to assess the straylight rejection. Another method to obtain such in-flight curves is to consider a horizontal strip obtained by averaging over ± 50 pixels (Figure 9b) around the central line to reduce statistical fluctuations when endeavouring to assess the instrumental solar straylight.

Figure 10 shows the comparison of the theoretical estimate of the straylight with the in-flight computed straylight from -0.25-arcdeg off-point images of 2010, along the central

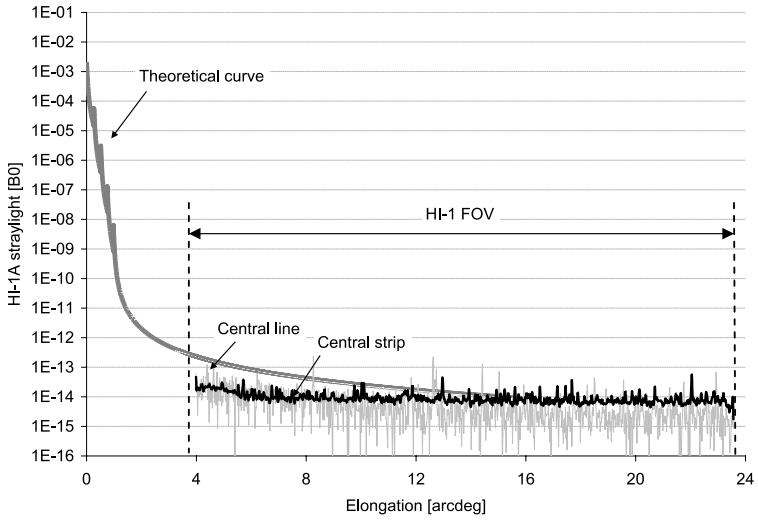

Figure 10 HI-1A straylight level for the −0.25-arcdeg pitch off-point captured in May 2010, quoted in units of B_0, along both the horizontal center line and the central strip, compared with the theoretical straylight curve, plotted as function of the elongation.

line and the central strip, expressed in units of B_0 and plotted as function of the elongation (defined from the center of the Sun).

The measured in-flight straylight is well below the theoretical prediction, showing the good performance of the instrument baffle system but also that the major predicted contributor to the HI-1 straylight is indeed the Sun. It also shows that the average lens barrel rejection factor taken into account in the theoretical curve is a worst case, as the lens barrel rejection pattern for an out-of-field light source (*i.e.* here the last edge of the front baffle) is probably not uniformly distributed over the detector. Nevertheless, no measurement has been made that would allow us to refine the out-of-field lens barrel rejection and the assumed value should be kept.

Figure 10 also indicates that the horizontal central strip curve is, as expected, much less noisy but still follows the horizontal central line curve closely, and can therefore be used for comparison with theoretical straylight.

As shown in Figure 11a, the straylight curve obtained at +0.5 arcdeg is very similar to the one obtained with the nominal science images (0-arcdeg off-point). Figure 11 shows that the straylight at +0.5-arcdeg off-point away from the Sun is not much less than at −0.5-arcdeg off-points toward the Sun. Straylight is thus not completely removed by the background subtraction, and what is measured at this offset is really straylight.

Figure 12 shows the comparison of theoretical straylight with in-flight straylight for the HI-1A and HI-1B off-point images from May 2010, calculated along the central strip, expressed in B_0 unit and plotted as a function of the elongation. The straylight level logically increases with increasingly negative off-pointing angle.

Figure 12 also shows that the straylight along the center strip is very similar for both HI-1A and HI-1B, as shown in detail in Figure 14a for the −0.25-arcdeg off-pointing angle as measured in May 2010. The same is true at all off-pointing angles except for the ring pattern intensity, as shown in Figure 14b for the largest angle (−1.25 arcdeg), which is slightly higher in HI-1B. This difference of ring pattern intensity is probably due to a difference in HI-1A and HI-1B lens barrel internal coatings.

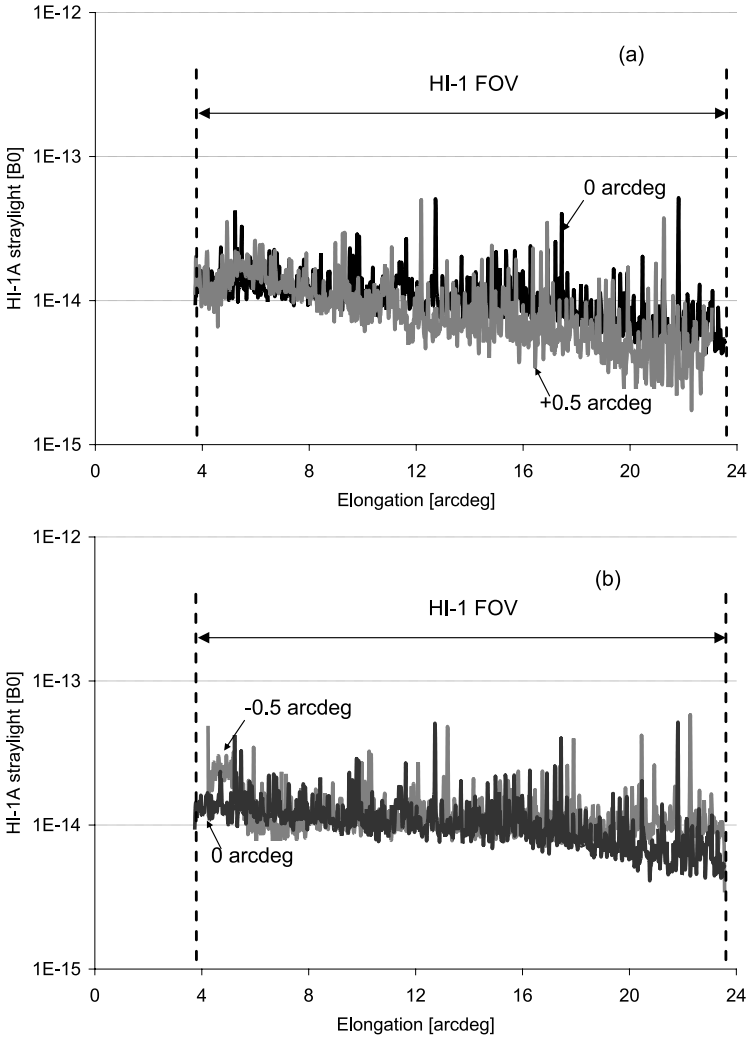

Figure 11 HI-1A straylight level along horizontal central strip (a) for the +0.5-arcdeg pitch off-point as compared with 0 arcdeg, and (b) for the −0.5-arcdeg pitch off-point as compared with 0 arcdeg, from May 2010 and quoted in units of B_0, plotted as function of the elongation.

Figure 12 also reveals that an additional straylight component is present in the images, albeit fainter in HI-1A than in HI-1B, which is not due to the sunlight diffracted by the front baffle system. A small bump is indeed present for all off-pointing angles but is more important for larger off-pointing angles. It corresponds to the ring-shaped pattern visible in Figure 3e and Figure 3f, which is produced by reflections within the HI-1 lens barrel, as described further in the present paper.

Figure 13 provides a comparison between the predicted diffraction curves and the measured straylight level in HI-1B images, at various off-point angles. At the smaller off-points the measurements are of a similar magnitude to the predicted diffraction (which assumes a factor of 10^{-2} for the lens barrel rejection), but at the larger off-points the measured curve

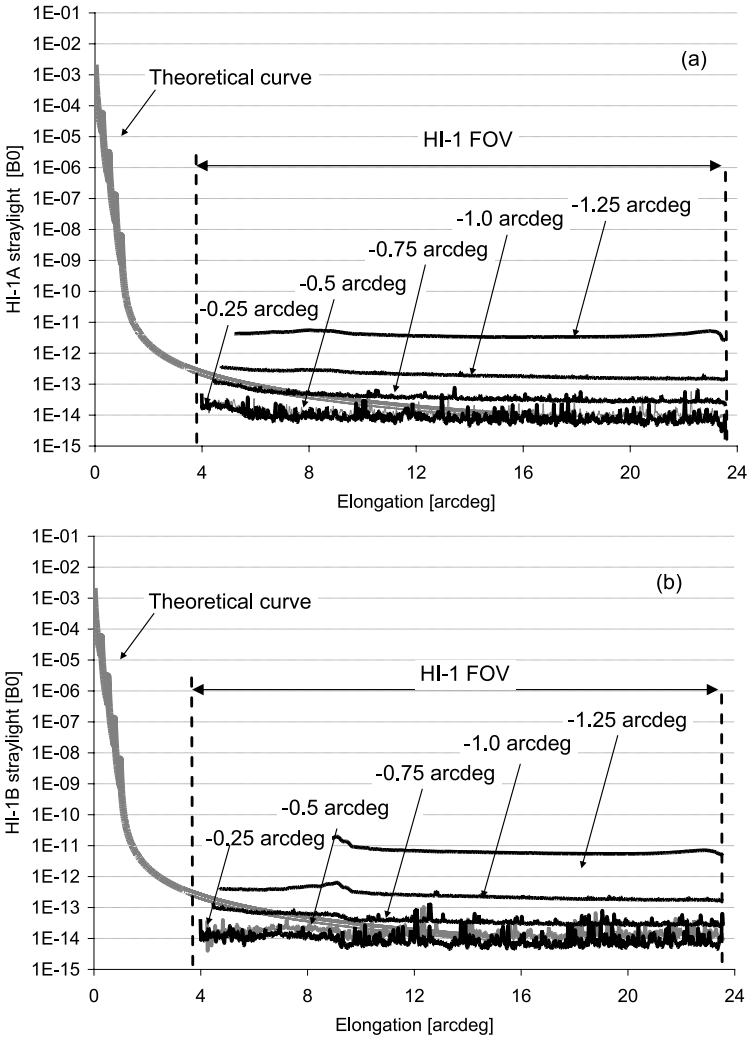

Figure 12 HI-1A (a) and HI-1B (b) straylight level, quoted in units of B_0, along the horizontal central strip, for increasing off-pointing images captured in May 2010 and compared with the theoretical straylight curve, plotted as function of the elongation.

lies significantly above the prediction, which is consistent with additional reflections within the lens barrel.

3.1.3. HI-1 Straylight Evolution

The straylight along the horizontal center strip as observed by HI-1A shows only a minor change from 2007 to 2010 for all off-points angles, as shown in Figure 15a for − 0.25 arcdeg and in Figure 15b for − 1.0 arcdeg (the largest common off-point angle in 2007 and 2010). This indicates that the efficiency of the front baffle, and hence the quality of the knife edges, has not been degraded over the three first years of the mission.

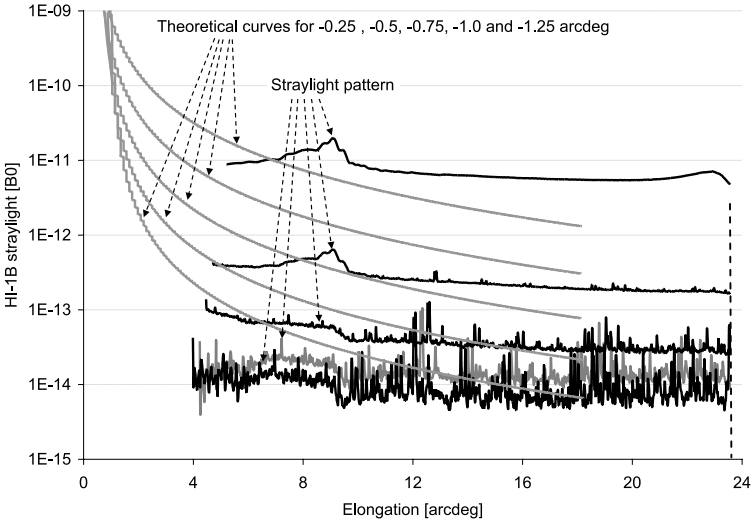

Figure 13 Detail of the HI-1B straylight levels along the horizontal central strip, for increasing off-pointing images, from May 2010, quoted in units of B_0 and plotted as a function of the elongation, revealing an additional straylight pattern.

Table 2 HI-1 maximum straylight (in B_0 units) at 0 arcdeg and -0.25 arcdeg, along with the requirement value.

	Requirement	0 arcdeg		-0.25 arcdeg	
		2007	2010	2007	2010
HI-1A	3×10^{-13}	2.4×10^{-14}	5.0×10^{-14}	5.9×10^{-14}	5.6×10^{-14}
HI-1B		–	7.4×10^{-14}	–	8.1×10^{-14}

Investigation of HI-1B straylight evolution between 2007 and 2010 is not possible because of the presence of comet Mc-Naught in the off-pointed images taken in January 2007 (Fulle *et al.*, 2007). Nevertheless, the close similarity between the off-pointed images taken by HI-1A and HI-1B in 2010 (Figure 14a) suggests that straylight evolution for HI-1B is likely to be very similar to that for HI-1A.

3.1.4. HI-1 Straylight Requirement

The maximum values of the straylight level along the horizontal center strip, quoted in units of B_0, are given in Table 2 for HI-1A and HI-1B, for both 2007 and 2010. These values are derived from the 0-arcdeg off-point observations, *i.e.* the nominal instrument pointing. Also noted in Table 2 is the requirement value for the per pixel straylight level at the anti-sunward edge of the HI-1 field of view where the signal is the weakest (Eyles *et al.*, 2009); this is the same for HI-1A and HI-1B. The maximum straylight levels are one order of magnitude better than the requirement value, showing that the front baffle efficiency is well within the required level in the science images.

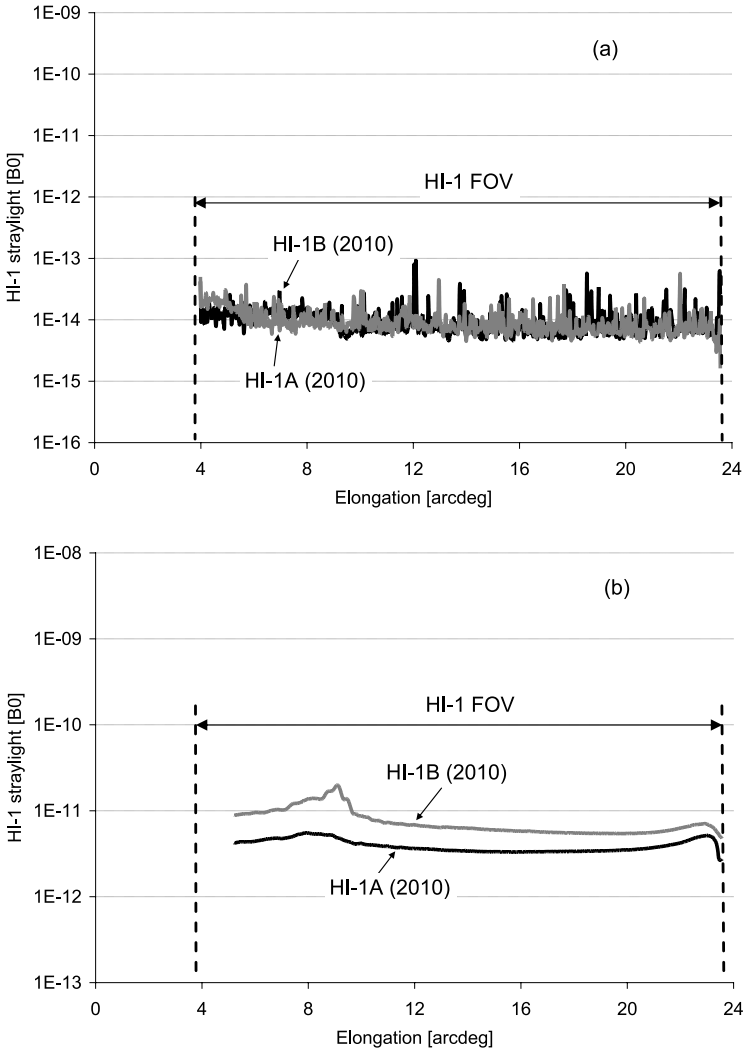

Figure 14 HI-1A and HI-1B straylight along the horizontal center strip (a) for the − 0.25-arcdeg off-pointing (b) for the − 1.25-arcdeg off-pointing from May 2010, quoted in units of B_0 and plotted as function of the elongation.

3.1.5. Straylight Ring Pattern

A ray-tracing model through the HI-1 camera optical system (Figure 16) shows that parasitic lens barrel reflections occur when there is a bright object close to but just outside the camera field of view. The resultant straylight in the image is a fixed ring-shaped pattern produced by a reflection on the last two retainers of the HI-1 lens barrel. The farther outside the field of view this light source is, the larger and less bright the ring pattern (Figure 17).

This effect arises wherever the bright source is located around the field of view, as the lens barrel is symmetric, but is most pronounced when the bright source is close to a corner of the detector. In fact, for the corners, the ring pattern is visible even when the bright source

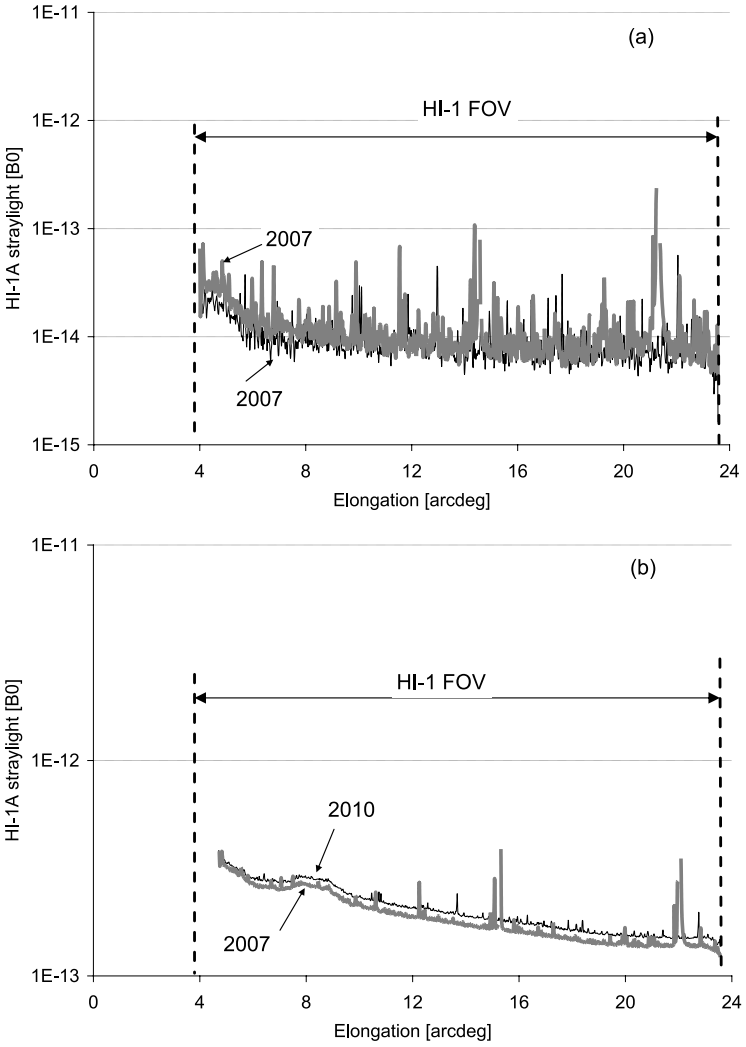

Figure 15 HI-1A straylight along the horizontal center strip, (a) for the − 0.25-arcdeg off-point, and (b) the − 1.0-arcdeg off-pointing angles from January 2007 and May 2010, quoted in units of B_0 and plotted as function of the elongation.

lies within the field of view, as shown in Figure 18, which is unexpected as it should only be imaged on the detector. This is due to the HI optical design, which has been optimized for a 10-arcdeg circular field of view and not for the square detector corners. As shown in Figure 19, the size of the ring pattern indeed reduces when the light source moves from the corner toward the center of the field of view.

The Sun can therefore produce such a ring pattern, as it is close to the edge of the camera field, which dominates the straylight for large negative off-points (Figure 3d and Figure 3e). Similarly, a ring pattern is also visible when a bright planet approaches the camera field of view (Figure 20), independently of the direction from which the planet approaches the field of view.

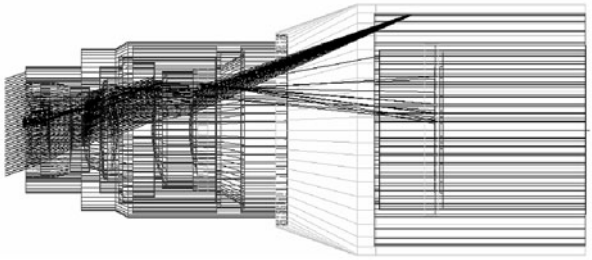

Figure 16 Ray-tracing model of a light source located just outside the edge of the HI-1 field of view, resulting in a ring-shaped straylight pattern.

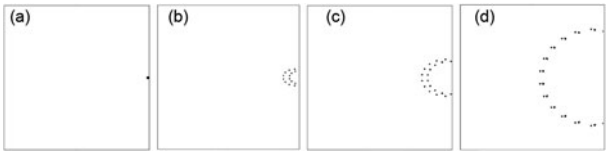

Figure 17 Simulated straylight ring pattern produced by a bright source located at 0 (panel a), + 3 (b), + 7 (c) and + 15 arcdeg (d) off the right-hand side of the HI-1 field of view.

Figure 18 Ray-tracing results for a bright source located in each of the four corners of the HI-1 field of view at 12.7 arcdeg from the field of view center.

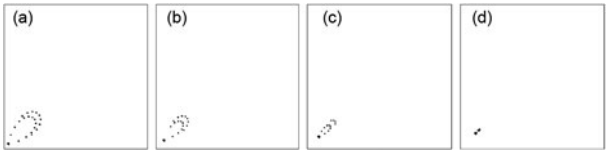

Figure 19 Ray-tracing results for a bright source located in the lower left corner of the HI-1 field of view at 13.4 arcdeg (panel a), 12.7 arcdeg (b), 12 arcdeg (c) and 11.3 arcdeg (d) from the field of view center.

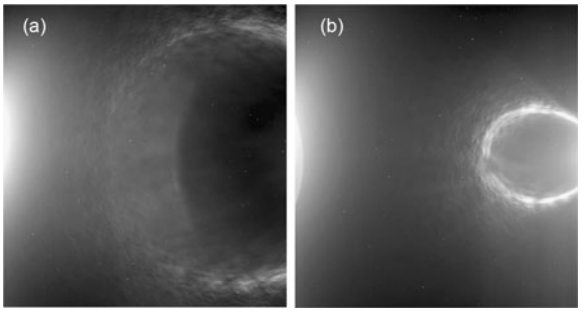

Figure 20 Straylight ring patterns in HI-1B images (with no background subtraction) produced by the Earth being just off the right-hand (anti-sunward) side of the field of view. At the times that these images were taken, the Earth was at (a) 30 arcdeg and (b) 26 arcdeg of elongation.

Using the HI-1 conversion factor given in Table 1 and the ray-tracing model, the ring pattern intensity can be quantified. The maximum straylight levels in the ring patterns (the background-subtracted images) formed by the Sun for an off-point of 1.5 arcdeg, by the Earth when located 2.35 arcdeg out of the field of view, and by Venus at the field of view border are given in Table 3.

Table 3 Straylight level (in B_0 units) in the HI-1 ring patterns.

Sun (with a 1.5 arcdeg off-point)	Earth (at 2.35 arcdeg out of field of view)	Venus (on field of view border)
5.4×10^{-11}	9.9×10^{-13}	2.7×10^{-13}

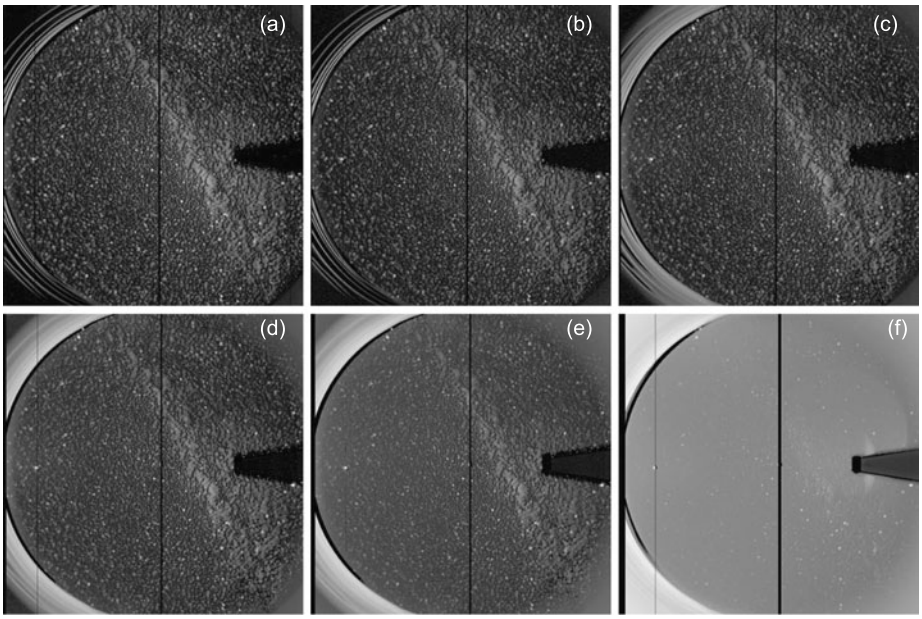

Figure 21 Background-subtracted HI-2B in-flight images from May 2010 for increasing pitch off-points (a) 0 arcdeg (b) − 0.25 arcdeg (c) − 0.5 arcdeg (d) − 0.75 arcdeg (e) − 1.00 arcdeg (f) − 1.25 arcdeg. Negative off-points are toward the Sun which, here for HI-2B, is off the image's left-hand side.

3.2. HI-2 Straylight Analysis

3.2.1. Off-pointing Images

The HI-2 images have been processed using the same method that was done for HI-1. Figure 21 presents the off-pointed HI-2B background-subtracted images taken in 2010 showing the increase in straylight with increasing off-point angle, computed using the conversion of the results to B_0 performed using the in-flight values given in Table 1.

As compared with HI-1 curves shown in Figure 12, the horizontal central strip curves computed for HI-2 shown in Figure 22 are dominated by the bright objects within the field of view such, in particular in HI-2B, where Milky Way is present. The off-pointing effect is, however, also clearly visible.

The intensity along the horizontal central strip in the HI-2A image is $< 5 \times 10^{-15}$ B_0 across the entire field of view for the − 0.25-arcdeg off-pointing. In the case of HI-2B it is also $< 5 \times 10^{-15}$ B_0, except for the region with elongations ∼ 50 to 70 arcdeg where un-subtracted background from the Milky Way dominates the residual intensity.

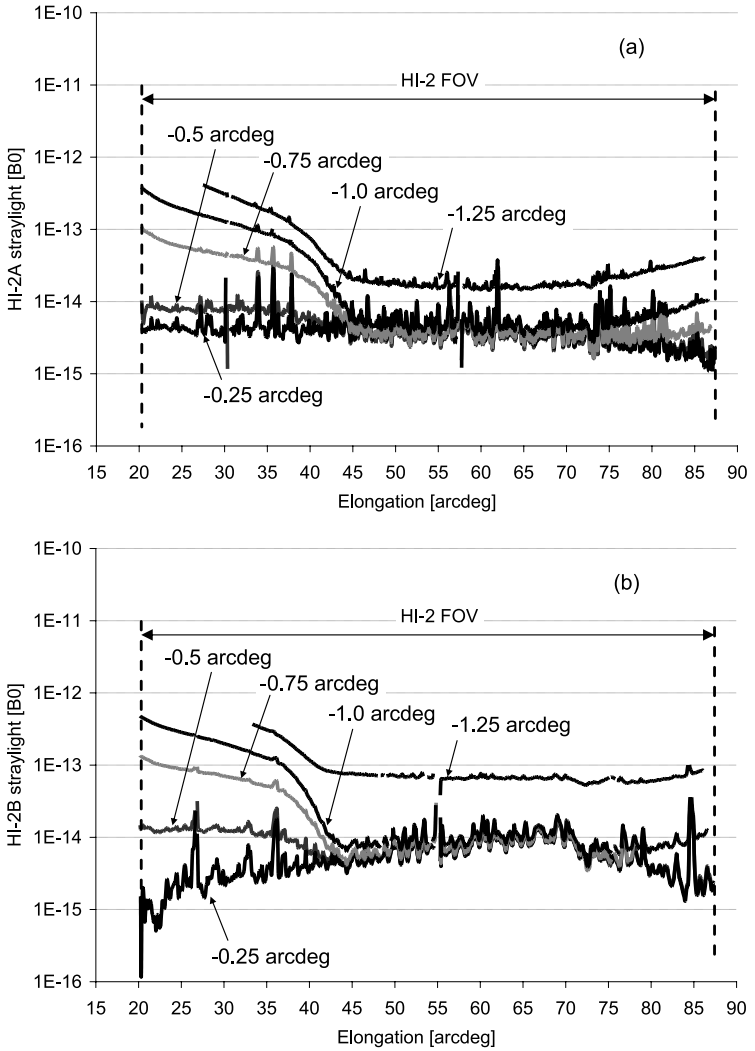

Figure 22 HI-2A (a) and HI-2B (b) straylight level, along the horizontal central strip, for increasing off–pointing images captured in May 2010, quoted in units of B_0, plotted as function of the elongation.

The intensity at a fixed elongation (taking into account the off-point) logically increases with increasingly negative off-point. For the largest off-point angle, *i.e.* -1.25 arcdeg, the image is clearly dominated by solar straylight (Figure 21e).

Based on these plots, and similar to the HI-1 results, the straylight level in HI-2A and HI-2B is summarized in Table 4, along with the requirement values. The overall straylight is well below the requirements level of 1×10^{-14} B_0 (Eyles *et al.*, 2009), for both HI-2A and HI-2B (as shown on Figure 23b) and has been stable since 2007 (as shown in Figure 23a).

Table 4 HI-2 average overall straylight in units of B_0, along with the HI-2 straylight requirement (Eyles *et al.*, 2009).

	Requirement	0 arcdeg		− 0.25 arcdeg	
		2007	2010	2007	2010
HI-2A	1×10^{-14}	3.9×10^{-15}	3.1×10^{-15}	4.4×10^{-15}	3.8×10^{-15}
HI-2B		–	4.9×10^{-15}	–	4.8×10^{-15}

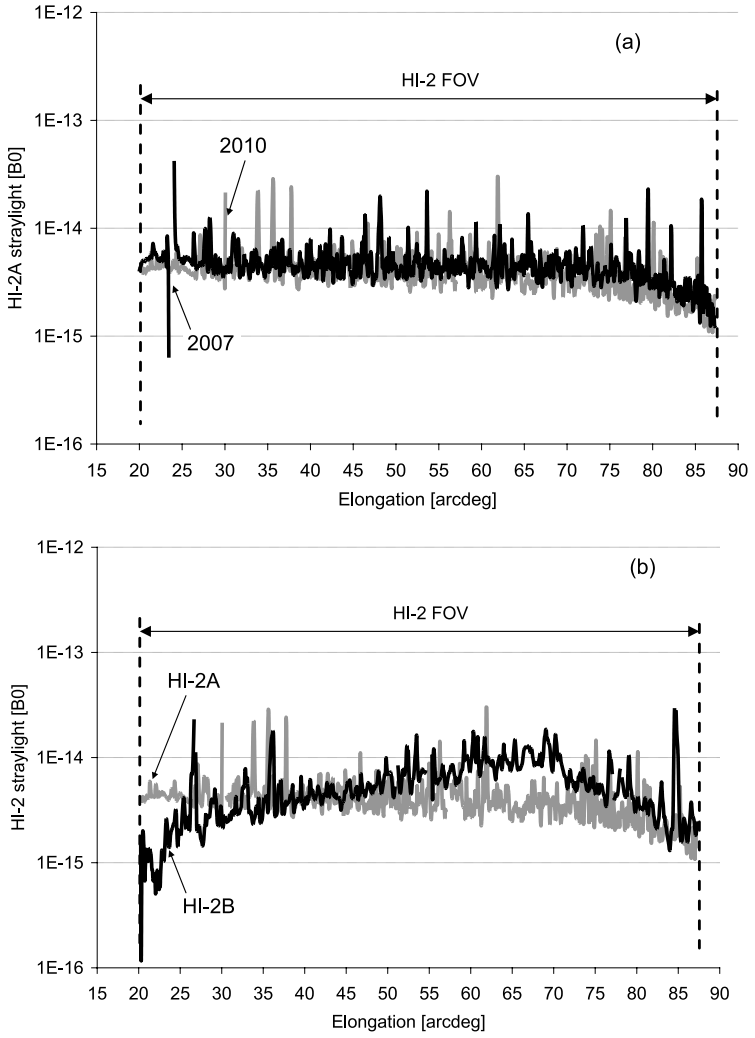

Figure 23 Comparison of straylight level at − 0.25-arcdeg off-point, along the horizontal central strip and quoted in units of B_0, plotted as function of the elongation, (a) for HI-2A images taken in January 2007 and May 2010, (b) for HI-2A and HI-2B images taken in May 2010.

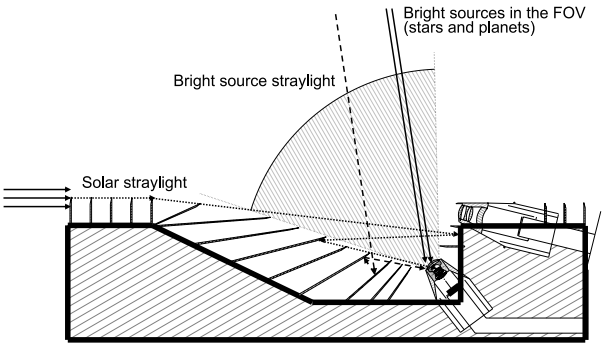

Figure 24 Straylight sources in HI-2 camera: straylight from the Sun and from bright sources located in the field of view.

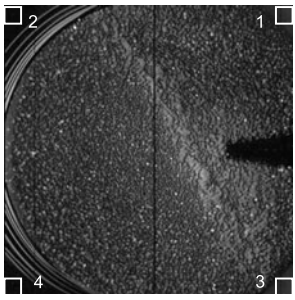

Figure 25 Definition of the image corners in the HI-2 straylight analysis. Corners 1 and 3 are those on the anti-sunward edge of the field of view, whereas corners 2 and 4 are on the sunward edge. The Sun is located on left-hand side of this HI-2B image.

3.2.2. Straylight Evolution in HI-2 Images

The straylight in HI-2 images is a combination of solar straylight and of diffuse straylight from the internal baffling reflecting bright objects facing the instrument (stars and planets) toward the HI-2 camera, as shown on Figure 24.

To track the evolution of the straylight in the HI-2 images, the method that has been used is based on the intensity in 50×50 pixels image corners (Figure 25) and on the average intensity over the entire field of view, assuming the straylight is uniformly spread over the entire field of view including the corners.

The sunward corners of the HI-2 images (2 and 4 as defined in Figure 22) are completely vignetted by the internal baffle and are imaging regions deep down in the internal baffle cavity. These corners are thus not illuminated by the bright sources within the field of view, and a signal in these corners thus stands as straylight (*i.e.* signal coming from an illuminated surface located out of the field of view). The anti-sunward corners of the HI-2 images (1 and 3 as defined in Figure 22) are partially vignetted within the HI-2 optics, being outside the nominal 35-arcdeg field of view, and their signal thus includes light from in-field objects.

The straylight evolution in the HI-2A and HI-2B corners has thus been monitored over the first three years of the mission using non-binned (2048×2048) images taken in nominal pointing (no off-point). The evolution of HI-2A and HI-2B corner averages is shown in Figure 26 as a function of time over the first three years of the mission. Figure 26 shows that the signal level in the corners varies with the bright objects passing through the field of view (planets like Venus and Mars, the Milky Way), which confirms that these corners are a good indicator of the straylight from in-field bright objects. In particular, Figure 26b shows that the straylight in HI-2B was dominated by the Earth during the first year of the mission (the Earth has subsequently reentered the field of view but is much fainter due to it being

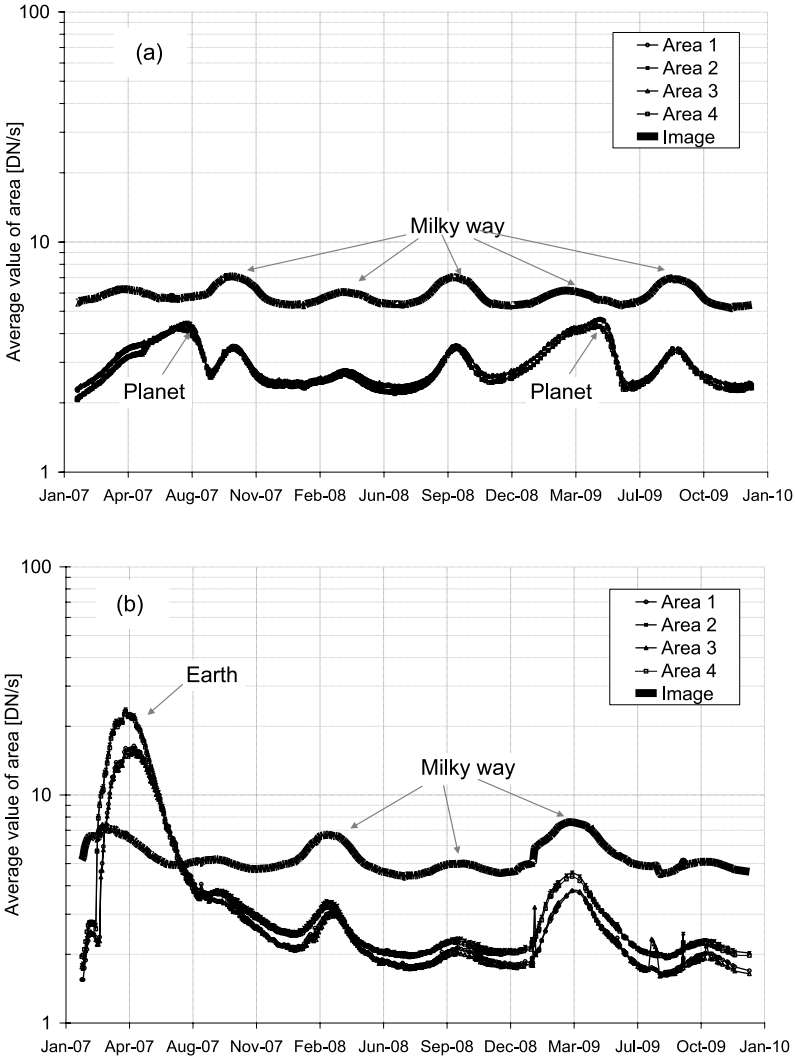

Figure 26 Straylight level evolution over time in HI-2A (a) and HI-2B (b) corners and entire image, for nominal-pointing image and quoted in DN s^{-1}.

much further from the spacecraft). For both HI-2A (Figure 26a) and HI-2B (Figure 26b), the regular transit of the planets and of the Milky Way through the field of view is clearly visible.

One method to highlight the straylight sources in the HI-2 field of view is to normalize the corner's average values with respect to the image average using the following relationship, as shown in Figure 27.

$$\text{Value}_{\text{Normalised}} = \frac{\text{Corner}_{\text{average}}/\text{image}_{\text{average}}}{\max(\text{Corner}_{\text{average}}/\text{image}_{\text{average}})}.$$

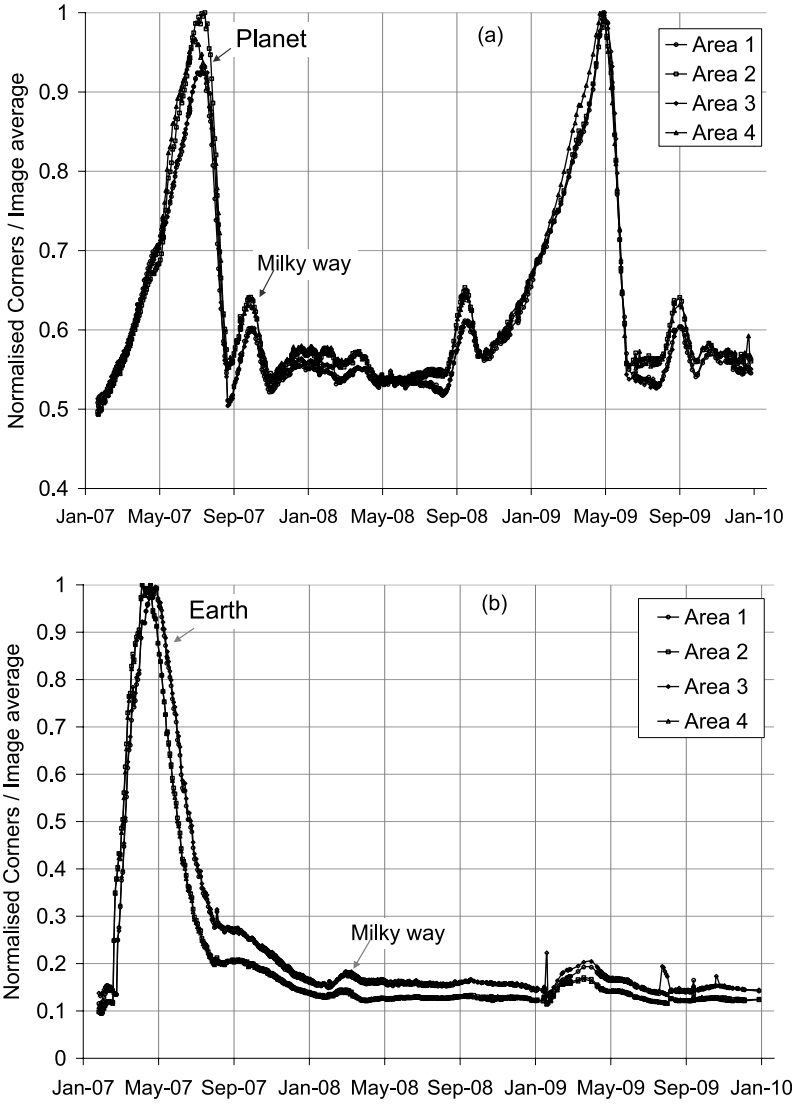

Figure 27 Normalized straylight level evolution over time in HI-2A (a) and HI-2B (b).

3.2.3. Other Possible Straylight Sources

Apart the solar straylight, visible in the off-pointed images, and the diffuse straylight from bright stellar object facing the instrument, another straylight source that was considered during the HI instrument design is the SWAVES boom antenna being located out of but close to the HI-2 field of view (Defise *et al.*, 2001) and that may have reflected the solar light toward the HI baffling system.

If not properly attenuated, this straylight source would have produced a straylight level in HI-2, and in particular in corners 2 and 4, which would have been a major contributor to the straylight level similar to bright planets (Defise *et al.*, 2002). The present analysis

confirms that the internal HI baffling is acting as designed and properly attenuates the boom straylight.

4. Conclusions

Accurate HI-1 and preliminary HI-2 in-flight image-based conversion factors have been used to express the straylight levels in HI-1 and HI-2 and their evolution over three years. It has been shown that the HI-1 straylight is unchanged after three years of operation and that it is principally composed of the solar light diffracted by the front baffle and of lens barrel internal reflection of bright objects located close to the edge of the field of view. The straylight level in HI-2 is dominated by bright objects such as the Earth and other planets, as well as the Milky Way, within the field of view. The levels of straylight for both HI-1 and HI-2 are well within the requirements, again showing the excellent performance and stability of the instrument baffling systems.

From our heritage with STEREO HI, a similar instrument for the ESA *Solar Orbiter* mission is under development. The present results are therefore important as they demonstrate the correspondence of the theoretical models with the in-flight straylight measurements and provide confidence in the baffling systems. They also show that an optimization of the lens barrel and of the detector cavity must be performed to limit internal lens barrel reflection, which is a non-negligible source of straylight.

Acknowledgements The Heliospheric Imager (HI) instrument was developed by a collaboration which included the University of Birmingham (UB) and the Rutherford Appleton Laboratory (RAL), both in the UK, the Center Spatial de Liège (CSL), in Belgium, and the Naval Research Laboratory (NRL), in the US. We thank the US institutions, funded by NASA; the UK institutions, funded by PPARC; and the Belgian institutions, funded by BELSPO. We also thank the referees and the editor for their constructive comments.

References

Bewsher, D., Brown, D.S., Eyles, C.J., Kellett, B.J., White, G.J., Swinyard, B.: 2010, *Solar Phys.* **264**, 433.
Brown, D.S., Bewsher, D., Eyles, C.J.: 2008, *Solar Phys.* **254**, 185.
Defise, J.-M., Halain, J.-P., Mazy, E., Rochus, P., Howard, R.A., Moses, J.D., Socker, D.G., Simnett, G.M., Webb, D.F.: 2001, *Proc. SPIE* **4498**, 63.
Defise, J.-M., Halain, J.-P., Mazy, E., Rochus, P., Howard, R.A., Moses, J.D., Socker, D.G., Harrison, R.A., Simnett, G.M.: 2002, *Proc. SPIE* **4853**, 12.
Eyles, C.J., Harrison, R.A., Davis, C.J., Waltham, N.R., Shaughnessy, B.M., Mapson-Menard, H.C.A., Bewsher, D., Crothers, S.R., Davies, J.A., Simnett, G.M., Howard, R.A., Moses, J.D., Newmark, J.S., Socker, D.G., Halain, J.-P., Defise, J.-M., Mazy, E., Rochus, P.: 2009, *Solar Phys.* **254**, 387.
Fulle, M., Leblanc, F., Harrison, R.A., Davis, C.J., Eyles, C.J., Halain, J.-P., Howard, R.A., Bockelee-Morvan, D., Cremonese, G., Scarmato, T.: 2007, *Astrophys. J. Lett.* **661**, L93.
Halain, J.P., Mazy, E., Defise, J.M., Moses, J.D., Newmark, J.S., Korendyke, C.M., Eyles, C.J., Harrison, R.A., Davis, C.J.: 2007, *Proc. SPIE* **6689**, 2.
Howard, R.A., Moses, J.D., Vourlidas, A., Newmark, J.S., Socker, D.G., Plunkett, S.P., Korendyke, C.M., Cook, J.W., Hurley, A., Davila, J.M., Thompson, W.T., St. Cyr, O.C., Mentzell, E., Mehalick, K., Lemen, J.R., Wuelser, J.P., Duncan, D.W., Tarbell, T.D., Wolfson, C.J., Moore, A., Harrison, R.A., Waltham, N.R., Lang, J., Davis, C.J., Eyles, C.J., Mapson-Menard, H., Simnett, G.M., Halain, J.P., Defise, J.M., Mazy, E., Rochus, P., Mercier, R., Ravet, M.F., Delmotte, F., Auchere, F., Delaboudiniere, J.P., Bothmer, V., Deutsch, W., Wang, D., Rich, N., Cooper, S., Stephens, V., Maahs, G., Baugh, R., McMullin, D., Carter, T.: 2008, *Space Sci. Rev.* **136**, 67.
Kaiser, M.L., Kucera, T.A., Davila, J.M., St. Cyr, O.C., Guhathakurta, M., Christian, E.: 2008, *Space Sci. Rev.* **136**, 5.
Mazy, E., Halain, J.-P., Defise, J.-M., Ronchain, P., Howard, R.A., Moses, J.-D., Eyles, C., Harrison, R.: 2005, *Proc. SPIE* **5962**, 509.
Neckel, H., Labs, D.: 1984, *Solar Phys.* **90**, 205.
Pickles, A.J.: 1998, *Publ. Astron. Soc. Pac.* **110**, 749.